
Article:
Anderson, M.J. orcid.org/0000-0001-5552-4459, Liao, L. and Basoalto, H.C. (2022) An assessment of statistical models of competitive growth during transient Ostwald ripening in turbine disc nickel-based superalloys. Modelling and Simulation in Materials Science and Engineering, 30 (7). 075005. ISSN 0965-0393

https://doi.org/10.1088/1361-651x/ac8c5d

An assessment of statistical models of competitive growth during transient Ostwald ripening in turbine disc nickel-based superalloys

OPEN ACCESS
IOP Publishing
Modelling and Simulation in Materials Science and Engineering
Modelling Simul. Mater. Sci. Eng. **30** (2022) 075005 (23pp) https://doi.org/10.1088/1361-651X/ac8c5d

An assessment of statistical models of competitive growth during transient Ostwald ripening in turbine disc nickel-based superalloys

M J Anderson[1,*], L Liao[2] and H C Basoalto[1]

[1] Department of Materials Science & Engineering,
The University of Sheffield, Mappin Street, Sheffield S1 3JD, United Kingdom
[2] School of Power and Mechanical Engineering, Wuhan University,
Wuhan, 430072, People's Republic of China

E-mail: M.J.Anderson@sheffield.ac.uk

Received 15 May 2022, revised 6 August 2022
Accepted for publication 24 August 2022
Published 8 September 2022

Abstract

The ability to accurately predict the time evolution of precipitate size distributions is fundamental to optimising heat treatments and mechanical properties of engineering alloys. Mean-field models of the particle growth rates assume that diffusion fields between neighbouring particles are weakly coupled reducing the problem to a single particle embedded in an effective medium. This regime of behaviour is expected to be satisfied for low volume fraction alloys. However, these assumptions are not fulfilled in many applications of interest where strong interactions between precipitates holds. Correction factors are often introduced to account for the accelerated rate of diffusion caused by the overlapping of diffusion fields between neighbouring precipitates. This paper applies the Wang–Glicksman–Rajan–Voorhees (WGRV) discrete point-source/sink model to compare descriptions of competitive growth. This includes assessing correction factors to the mean-field particle growth rate derived by Ardell, Marqusee and Ross, and Svoboda and Fischer in addition to Di Nunzio's pairwise interaction model. The WGRV model is used as a benchmark to compare different approximations of competitive growth that apply similar assumptions. This is followed by the application of the models to simulate precipitation kinetics during long term aging kinetics observed in the nickel-based

*Author to whom any correspondence should be addressed.

superalloys IN738LC and RR1000. It is shown that the competitive growth correction factors are accurate for volume fractions of 20% and under-predict the acceleration of precipitate kinetics predicted at 40%. The WGRV model is able to capture the coarsening kinetics observed in both IN738LC and RR1000 with reasonable accuracy. The WGRV model determines particle growth rates as a function of the immediate neighbourhood and provides an improved prediction of the coarsening behaviour of tertiary particles in RR1000 in comparison to the mean-field approximation, however over-estimates the growth rate of the tertiary particles compared to experimental data.

Keywords: mean-field modelling, precipitation, nickel superalloys, competitive growth, particle coarsening, transient Ostwald ripening

(Some figures may appear in colour only in the online journal)

1. Introduction

Plastic deformation of nickel-based superalloys is sensitive to the size, volume fraction, and spatial arrangement of strengthening precipitates. In the turbine-disc nickel-superalloys RR1000 and IN738LC, the intermetallic γ' phase is the strengthening precipitate with an equilibrium volume fractions of approximately 45% in the as-heat treated condition. Heat treatments in these alloys are carefully designed to generate multi-modal γ' dispersions to optimise in-service creep and fatigue performance. However, under in-service conditions these alloys are exposed to temperatures sufficient to continue the coarsening of the precipitate dispersion, impacting properties and component performance. It is often possible to predict qualitative mechanical behaviour utilising statistical models of precipitation assuming that kinetics are driven solely by Ostwald ripening, where precipitates grow to minimise the Gibbs free energy of the system by reducing the total surface area of the dispersion [1, 2]. These approaches use mean-field descriptions of the precipitate growth rate for predicting the evolution of the particle size distribution, where the many-particle problem is reduced to a one-particle problem embedded in an effective medium. These methods are attractive in that they reduce the complexities of solving mass transport and mechanical filed equations governing interactions between multi-component diffusion and mechanical fields. They simulate the evolution of the size distribution of precipitates, providing information regarding the volume fraction and mean radius which may be used to approximate inter-particle spacing and mechanical properties [3, 4]. However, limitations arising from the simplifying assumptions made in the derivation of these models impacts the ability to make quantitatively accurate predictions. To overcome these limitations, mean-field descriptions need to be extended with additional physics that justifies their application to regimes were weak coupling of diffusion fields is no longer applicable.

The nucleation, growth, coarsening, and dissolution of precipitates in nickel superalloys can be rationalised through energy minimisation and the kinetics of diffusion of the precipitate forming species. Ostwald ripening refers to coarsening behaviour driven by interfacial energy minimisation of the precipitates. Greenwood [5], Lifshitz and Slyozov [6], and Wagner [7] developed the first descriptions of mean-field particle coarsening for dilute concentration binary alloys. In their treatment, a number of simplifying assumptions are made and include: spherical particles, no interactions between the diffusion and elastic fields between precipitates, no coalescence and negligible spatial variation of composition within

the alloy. In non-dilute alloys, the diffusion fields surrounding precipitates overlap, increasing the spatial concentration gradient of the solute, and thus accelerates diffusion and particle growth kinetics. Correction factors have been introduced to the particle growth rate to better account for finite size particles and interactions though their diffusion fields. This is referred to as competitive growth and is the focus of this paper which verifies the self-validity of several correction factors and then assesses to what extent capturing competitive growth improves accuracy when modelling isothermal aging in multi-modal engineering Ni-based superalloys.

Ardell [8] proposed a correction factor to the Lifshitz–Slyozov–Wagner (LSW) particle growth rate by considering a diffusion screening length that was approximated by half of the mean particle spacing. Tsumuraya and Miyata [9] and Wang *et al* [10] explored different approximations of the diffusion screening length with recent contributions from Glicksman *et al* [11] and Svoboda and Fischer [12]. Di Nunzio [13] has derived a statistical particle growth model to capture competitive growth more accurately by considering pairwise interactions between particles of different size classes. The form of Di Nunzio's particle growth rate differs from the conventional LSW particle growth rate, deriving an integro-differential equation for the particle growth rate.

Marqusee and Ross (MR) [14], Voorhees and Glicksman [15], and Hayakawa and Family [16] approached the multiple-particle diffusion problem by treating a discrete set of particles as point sources or sinks of solute within a quasi-static diffusion field, and derived correction factors for the LSW particle growth rate. These discrete particle descriptions capture the impact of the overlap in diffusion fields as a function of the size and spatial arrangement of the particles. Wang *et al* [17] have developed a discrete particle coarsening model which builds upon the work of Voorhees and Glicksman [15]. This model is referred to as the Wang–Glicksman–Rajan–Voorhees (WGRV) model. The WGRV model has been applied to test different statistical approximations of competitive growth and predict particle coarsening in a multi-modal particle system. The comparison verifies the suitability of the competitive growth correction factors to models derived using the same assumptions regarding the diffusion fields and particle morphology.

Mean-field models of precipitation predict that any starting dispersion will evolve towards an attractor state, where the shape of the particle size distribution remains invariant with time. Upon reaching the attractor state, scaling laws emerge that describe the continued coarsening of the dispersion. Chen and Voorhees [18] describe these regimes as the transient and steady-state regimes of Ostwald ripening. Previous studies have focused on developing improved descriptions of competitive growth during the steady-state coarsening regime of system with finite volume fractions of precipitates [12, 13, 17]. These studies provide valuable insights into coarsening behaviour at long time scales, however, in the nickel-based superalloys of interest the dispersions would be over-aged once they reach the steady-state regime. This work focuses on studying competitive growth behaviour during the transient coarsening regime where the dispersions provide optimum mechanical properties and kinetics are of most importance considering component performance. The mean-field and WGRV models have been applied to study their ability to predict coarsening kinetics in the multi-component nickel-based superalloys IN738LC [19] and RR1000 [20]. The paper provides the following contributions;

- An assessment of statistical approximations of competitive growth.
- An evaluation of the WGRV model to predict coarsening kinetics of multi-modal precipitate dispersions in nickel-based superalloys.

- An algorithm for quickly generating high volume fraction polydisperse non-penetrating systems of spherical particles.

The paper is structured so that the next section introduces the models evaluated in the paper. The following section describes how they have been implemented. The model results are presented in section 4, evaluating descriptions of competitive growth, and then applying the models to predict kinetics in two nickel-based superalloys. The paper ends with discussion and conclusions, showing that the correction factors can predict similar behaviour when the volume fraction of the particle dispersion is less than 20%, and that the multi-particle WGRV model does improve the ability to accurately capture the evolution of multi-modal size distributions observed in aged IN738LC and RR1000.

2. Model formulation

Particles are treated as spherical with their growth rate a function of the particle size and composition. The particle dispersion is described by the particle radius distribution (PRD) function $\mathcal{F}(R,t)\mathrm{d}R$, which describes the number of particles of size R in the interval $R + \mathrm{d}R$ per volume at a given time, t. The dispersion parameters of interest are calculated from moments of $F(R,t)$. By definition, the Dth moment of $\mathcal{F}(R,t)\mathrm{d}R$ is given by

$$M^{(D)} = \int_0^\infty \mathcal{F}(R,t)R^{(D)}\,\mathrm{d}R. \tag{1}$$

The particle concentration $N_v(t)$, mean radius $\langle R(t)\rangle$ and volume fraction $\phi(t)$ are related to these moments as follows

$$\begin{aligned} N_v(t) &= M^{(0)} \\ \langle R(t)\rangle &= M^{(1)}/M^{(0)} \\ \phi(t) &= \frac{4\pi}{3}M^{(3)} \end{aligned} \tag{2}$$

The evolution of the particle distribution is determined by the continuity equation

$$\frac{\partial \mathcal{F}(R,t)}{\partial t} + \frac{\partial \mathcal{F}(R,t)V(R,t)}{\partial R} = \mathcal{F}^+(R,t) - \mathcal{F}^-(R,t), \tag{3}$$

where the terms $\mathcal{F}^+(R,t)$ and $\mathcal{F}^-(R,t)$ refer to source and sink rate terms. $\mathcal{F}^+(R,t)$ includes particle nucleation, and $\mathcal{F}^-(R,t)$ describes the removal of particles through dissolution. During coarsening it is assumed that $\mathcal{F}^+(R,t) = 0$. The particle growth rate is given by $V(R,t)$, where LSW style growth rates have the following general form [21]

$$V(R,t) = \frac{A(t)}{R}\left(\frac{1}{R_\mathrm{c}(t)} - \frac{1}{R}\right)z(R,t), \tag{4}$$

where $A(t)$ includes information on diffusion mobilities of alloying elements at the particle-matrix interface. The approximation for $A(t)$ in binary alloys is given by

$$A(t) = \frac{D\gamma V_\mathrm{m} c_0}{R_\mathrm{g}T}, \tag{5}$$

where D is the diffusivity of the precipitate forming solute, V_m is the molar volume, c_0 is the equilibrium molar concentration of solute in the matrix, R_t is the gas constant, and T is

the absolute temperature. The term $R_c(t)$ is a critical particle radius, such that particles with a smaller radius than this value will dissolve and larger ones will grow. During coarsening, $R_c(t)$ is given by [20]

$$R_c = \frac{\int_0^\infty \mathcal{F}\, R\, z\, \mathrm{d}R}{\int_0^\infty \mathcal{F}\, z\, \mathrm{d}R} \tag{6}$$

The $z(R,t)$ term in equation (4), is a correction factor accounting for the impact of the overlap of diffusion fields between neighbouring particles which accelerate particle growth kinetics. Many authors have developed approximations for the $z(R,t)$ factor [8, 9, 11, 12, 14–16, 22]. Ardell [8] approached the problem by considering a diffusion screening distance $R_0(t)$ based upon the Dirichlet region surrounding a particle and arrived at the following approximation

$$z(R,t) = 1 + \frac{R}{R_0(t)} \tag{7}$$

Ardell [8] approximated this distance by half of the mean particle spacing. The mean centre to centre distance between particles can be approximated by $1/N_v^{1/3}$. The problem can be simplified to a monodisperse system with the particle radius approximated by $\langle R\rangle$. The mean particle spacing $\langle\lambda\rangle$ within the matrix is thus

$$\langle\lambda\rangle = 1/N_v^{1/3} - 2\langle R\rangle \tag{8}$$

Continuing with the monodisperse approximation, the particle number concentration can be approximated by $(3\phi)/(4\pi\langle R\rangle^3)$, allowing for the mean matrix spacing to be given by

$$\langle\lambda\rangle = \langle R\rangle\left(\left(\frac{4\pi}{3\phi}\right)^{1/3} - 2\right) \tag{9}$$

Wang *et al* [10] tested several approximations of the particle spacing to spacings calculated from numerically generated dispersions and found that Bansal and Ardell's [23] approximation was most accurate. This work finds Lu and Torquato's [24] nearest neighbour distribution function a better description of the nearest particle spacing. Bansal and Ardell's [23] particle spacing calculation is

$$\langle\lambda\rangle = \langle R\rangle\left(2 + \frac{\exp(8\phi)}{3\phi^{1/3}}\Gamma\left(\frac{1}{3}, 8\phi\right)\right), \tag{10}$$

where Γ is the incomplete gamma function. Several particle spacing descriptions have been evaluated, finding that Lu and Torquato's [24] nearest neighbour distribution functions best reproduces particle spacings and the kinetics predicted by the WGRV model. More information regarding Lu and Torquato's spacing calculation is given in section 6 of the appendix.

Glicksman *et al* [11] offer the following description for $R_0(t)$

$$R_0(t) = \frac{1}{\sqrt{3}}\left(\frac{M^3(t)}{M^1(t)},\right)^{1/2}\phi^{-1/2}(t), \tag{11}$$

where M^n is the nth moment of the PRD function. When equation (11) is used within equation (7), the result is mathematically equivalent to that of MR [14], who derived the following z factor expression after treating the particles as point sources and sinks with a quasi-static diffusion field,

$$z(R,t) = 1 + R\sqrt{4\pi M^1} \tag{12}$$

Svoboda and Fischer [12] and Wang and Glicksman [25] propose the following form for the $z(R,t)$ factor:

$$z(R,t) = \left(1 - \frac{R}{R_0(t)}\right)^{-1} \tag{13}$$

with the following approximation for $R_0(t)$ [12]:

$$R_0(t) = \frac{kR_c(t)}{\phi^{1/3}(t)}, \tag{14}$$

where the physical origin of k is the ratio of the lattice parameter and the Madelung constant. The $z(R,t)$ factors which share the form shown in equation (13) are suitable for describing coarsening kinetics during steady state coarsening regimes. These approximations suffer from numerical instability when applied to certain particle size distributions observed during transient coarsening kinetics as they cannot be applied to a particle of radius greater than R_0. This prohibits the use of Wang and Glicksman's z factor [25] to the multi-modal particle dispersions of interest in this work. Svoboda and Fischer's approximation may be used if the k term is chosen to ensure R_0 is greater than the largest particle present in the dispersion.

Di Nunzio [13] derived a model of competitive growth considering pair-wise interactions between the precipitate size classes present within the dispersion that has a different form to that shown in equation (4). Di Nunzio's particle growth rate may be reformulated to be expressed in terms of the PRD function $\mathcal{F}(R,t)$ following the steps outlined in the appendix A. This results in the following integro-differential equation

$$\begin{aligned}
V(R_i,t) &= \frac{A^*(t,R_i)}{R_i^2}\int_0^\infty \tilde{b}(R_j)\mathcal{F}(R_j,t)\left(\frac{1}{R_j} - \frac{1}{R_i}\right)\mathrm{d}R_j \\
\tilde{b}(R_i) &= \frac{\tilde{v}(R_i)}{\int_0^\infty F(R)\tilde{v}(R)\mathrm{d}R} \\
\tilde{v}(R_i) &= 1 + \alpha^2 M^0 \frac{R_i^2}{M^2}\frac{1}{\phi^{2/3}} \\
A^*(t,R_i) &= A(t)\tilde{b}(R_i)\frac{\phi^{1/3}}{1-\phi^{1/3}}\frac{M^2}{M^1}M^0
\end{aligned} \tag{15}$$

The term α is a characteristic parameter that defines the average effective inter-particle distance and has a value of 2.568 28. Note that the particle growth rate is proportionate to $1/R^3$ compared to the $1/R^2$ behaviour LSW style growth rates that share the form of equation (4).

2.1. The WGRV multi-particle model

The discrete particle WGRV model [17] calculates the concentration gradients explicitly and offers a more accurate description of competitive growth. It assumes a periodic ensemble of n

spherical particles, with centres located at $\boldsymbol{r}_i$ for $i = 1, 2, \ldots, n$. The model considers a binary alloy where $c(\boldsymbol{r})$ is the concentration of particle forming atoms at location $\boldsymbol{r}$. The equilibrium molar solute concentration of precipitate forming species in the matrix of the binary alloy is given by c_0. The local solute concentration is described using the following dimensionless diffusion potential

$$\varphi(\boldsymbol{r}) = \frac{c(\boldsymbol{r}) - c_0}{c_0} \tag{16}$$

The spatial and temporal dimensions are normalised by the capillary length l_c and τ respectively, which are given by $l_c = (2\gamma V_m)/(R_g T)$ and $\tau = l_c^2/(D c_0 V_m)$. By treating the particles as fixed-point sources or sinks, a form of Poisson's equation may be used to describe the evolution of a quasi-static approximation of the diffusion field

$$\nabla^2 \varphi(\boldsymbol{r}) = \sum_{i=1}^{m} -4\pi B_i \delta(\boldsymbol{r} - \boldsymbol{r_i}), \tag{17}$$

where $4\pi B_i$ is the total volume flux of the ith particle. Voorhees and Glicksman [15] explored the following solution to equation (17) representing a distribution of point sources and sinks:

$$\varphi(\overrightarrow{r}) = \sum_{i=1}^{n} \frac{B_i}{|\overrightarrow{r} - r_i|} + \varphi_\infty, \tag{18}$$

where φ_∞ is the far-field diffusion potential. It is assumed that during particle coarsening the volume fraction of particles is conserved such that $\sum B_i = 0$. The boundary condition $\varphi(R_i) = 1/R_i$ may be applied to equation (18), and B_i may be separated from the summation to obtain the following,

$$\frac{1}{R_i} = \frac{B_i}{R_i} + \sum_{k \neq i}^{n} \frac{B_k}{|r_i - r_k|} + \varphi_\infty \tag{19}$$

Through some algebra, it is possible to arrive at the following linear system of equations [22],

$$\sum_{k=1}^{n} B_k \left[\frac{1}{|r_i - r_k|} - \frac{1}{n\langle R \rangle} \sum_{i \neq k}^{n} \frac{R_i}{|r_i - r_k|} \right] = \frac{1}{R_i} - \frac{1}{\langle R \rangle} \tag{20}$$

The evolution of a particle dispersion may be calculated by solving equation (20) for B and then evolving the particle radius through the system of ordinary differential equations given by $\dot{R}_i = -B_i/R_i^2$.

3. Numerical implementation

The statistical precipitation models that solve kinetics through evolving the PRD function have been implemented by following the procedure described by Anderson *et al* [26], normalising both spatial and temporal dimensions, and then applying a volume fraction reformulation. The continuity equation shown in equation (3) is solved using a Hamilton–Jacobi ENO3 scheme [27].

The method described by Wang *et al* [17] has been followed to solve the discrete particle WGRV model. This involves solving the linear set of equations given in equation (20) using the Gauss–Seidel method and using Runge–Kutta to approximate the particle growth rate.

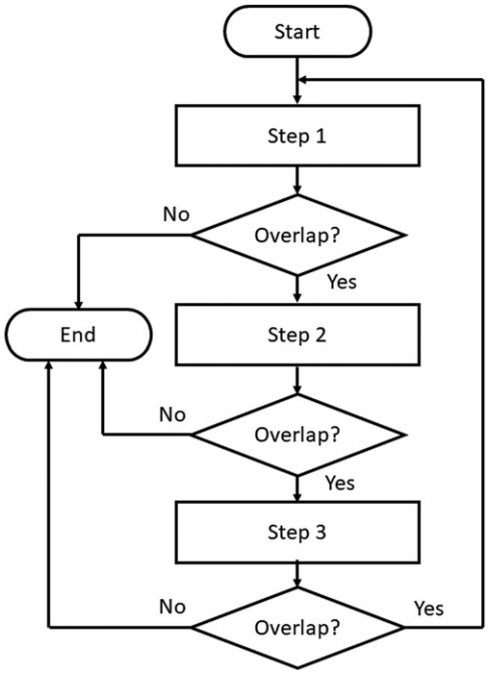

Figure 1. A flowchart describing the method used to generate random 3D polydisperse non-penetrating particle ensembles

A novel method has been developed for generating non-dilute random 3D polydisperse non-penetrating particle ensembles, utilising nearest neighbour distribution functions to inform guesses for the placement of particles. Lu and Torquato [24] generated random dispersions of spherical particles by first placing the particles on a regular lattice and then repeatedly moving particles a small distance in a random direction until the dispersion was sufficiently randomised. An alternative method has been developed that creates randomised non-dilute dispersions with less computation time. It involves multiple attempts at placing the particle within the ensemble and is described in figure 1. The particles to be positioned within the domain are placed into the volume in descending order of size. The workflow is described in figure 1 and the steps used are listed below:

- Step 1: a pseudo-random number generator is used to determine coordinates within the domain for an attempt to place the particle.
- Step 2: the previous method failed and the attempted location to position the next particle penetrated an existing particle within the ensemble. A vector is created between the attempted location and the penetrating particle's centre coordinates. The E_p function described in the appendix is used to determine a random matrix distance separating the next particle from the penetrating particle using the penetrating particle as the reference particle. This location is then used to attempt to place the particle.
- Step 3: the attempt to place the particle a distance away from the penetrating particle failed, encountering another particle. The two penetrating particles identified from methods 1 and 2 are noted, and the next closest particle to the attempted location to position the particles is identified. The centre point between these three particles is then computed, and the

Table 1. Model parameters for the WGRV and MR models.

Alloy	γ (J m^{-2})	V_m (m^3 mol^{-1})	Q (kJ mol^{-1})	D_0 (m^2 s^{-1})	C_0 (mol m^{-3})
IN738LC	0.03	7.44×10^{-6}	280	4×10^{-6}	4.032×10^3
RR1000	0.03	7.44×10^{-6}	290	2×10^{-5}	4.059×10^3

Table 2. Model parameters for the Di Nunzio model.

Alloy	γ (J m^{-2})	V_m (m^3 mol^{-1})	Q (kJ mol^{-1})	D_0 (m^2 s^{-1})	C_0 (mol m^{-3})
IN738LC	0.03	7.44×10^{-6}	270	2×10^{-4}	4.032×10^3
RR1000	0.03	7.44×10^{-6}	310	2×10^{-5}	4.059×10^3

distance to the closest particle at this location can then be calculated. If this distance is larger than the radius of the particle that is to be positioned, a random location within this region is chosen to place the particle.

The first particle is positioned randomly within the domain using step 1. The next particle is positioned using steps 1 and 2 iteratively until successful positioning of the particle. The algorithm shown in figure 1 is then applied to position the following particles to create the polydisperse ensemble. The procedure offers some simplifications to Lu and Torquato's [24] approach when creating randomly dispersed multi-modal populations of particles by avoiding the need to identify a suitable density of sub-lattices to position the smaller particles.

The calculations have been performed in normalised space for the isothermal heat treatments. The model parameters have been calibrated to the experimental data reported in [20, 27] when converting back to real space. The calibrated parameter-sets are presented in table 1 for the WGRV, MR, SF, and Ardell models, and table 2 Di Nunzio's model.

4. Results

4.1. Competitive growth

The WGRV model has been used to test different approximations of competitive growth. The particle ensembles needed for this model have been generated numerically, ensuring a random periodic dispersion of non-penetrating particles. The particle growth rates assessed are summarised below:

Marquesee and Ross (MR) [14] $$V(R) = \frac{A}{R}\left(\frac{1}{R_c} - \frac{1}{R}\right)\left(1 + R\sqrt{4\pi M_1}\right) \tag{21}$$

Svoboda and Fischer (SF) [12] $$V(R) = \frac{A}{R}\left(\frac{1}{R_c} - \frac{1}{R}\right)\left(1 + \frac{R\,\phi^{1/3}}{k\,R_c}\right)^{-1} \tag{22}$$

Ardell [8] $$V(R) = \frac{A}{R}\left(\frac{1}{R_c} - \frac{1}{R}\right)\left(1 + \frac{R}{R_0}\right) \tag{23}$$

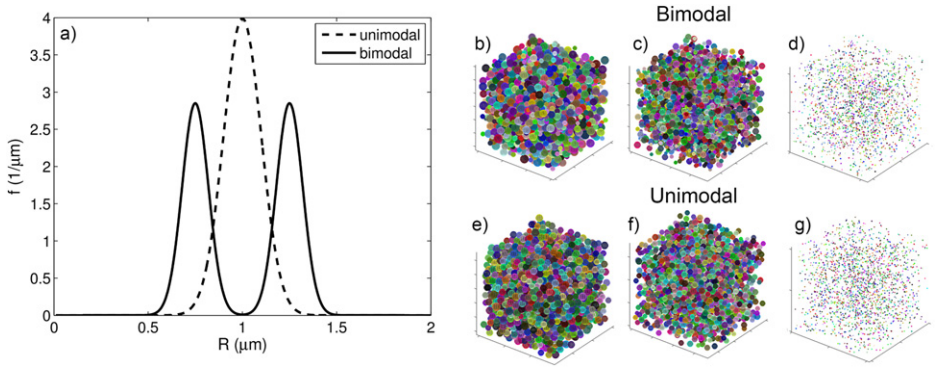

Figure 2. (a) The unimodal and bimodal particle radius probability distribution functions used to assess descriptions of competitive growth against the WGRV model. Figures (b)–(g) present examples of the 3D precipitate ensembles generated for use in the WGRV model. Figures (b)–(d) refer to the bimodal distribution, and figures (e)–(g) refer to the unimodal distribution as described in figure (a). Figures (b) and (e) have a volume fraction of 40%, figures (c) and (f) have 20%, and figures (d) and (g) have 0.1%.

Di Nunzio [13]
$$V(R_i) = \frac{A^*(R_i)}{R_i^2}\int_0^\infty \tilde{b}(R_j)\mathcal{F}(R_j)\left(\frac{1}{R_j}-\frac{1}{R_i}\right)\mathrm{d}R_j \quad (24)$$

The coarsening kinetics of a bimodal and unimodal particle dispersion with varying volume fractions have been calculated to test different approximations of the z factor to those obtained from the WGRV model. The particle size probabilities are calculated from the following normalised Gaussian PRD [18]

$$\begin{aligned}\chi(\rho, t=0) &= \frac{A}{\sigma\sqrt{2\pi}}\exp\left[\frac{-(\rho-\mu)^2}{2\sigma^2}\right]\\ \rho &= R/\langle R\rangle \\ \chi\mathrm{d}\rho &= \frac{4\pi}{\phi_\infty}FR_c^3\mathrm{d}r\end{aligned} \quad (25)$$

where μ and σ affect the shape of the size distribution and the normalisation constant A is determined from mass balance. The unimodal particle size distribution is generated using a μ parameter value of 1.0 and a σ value of 0.1. The bimodal distribution is generated using μ values of 0.75 and 1.25, and σ values of 0.07 and 0.25. Both particle size distributions had a mean particle size of 1 μm with volume fractions of either 40%, 20% or 0.1%.

Figure 2 presents the particle size probabilities and an illustration of the particle ensembles generated for the calculation. A typical simulation of the concentration fields predicted by the WGRV model is shown in figure 3, which compares the dimensionless diffusion potential, φ for a cross section of a system of particles.

Figures 3(a), (c) and (e) are obtained from a unimodal dispersion whilst (b), (d) and (f) are from the bimodal dispersion. Values of φ greater than unity refer to a source of solutes whilst a value lower is a sink. Particles which are solute sources are shrinking whilst particles that are solute sinks are growing. For the dilute particle dispersions ($\phi = 0.1\%$), the diffusion fields rarely overlap. The range in φ is larger in the bimodal particle dispersion than the unimodal dispersion for each volume fraction considered. The amount of overlap in φ increases with

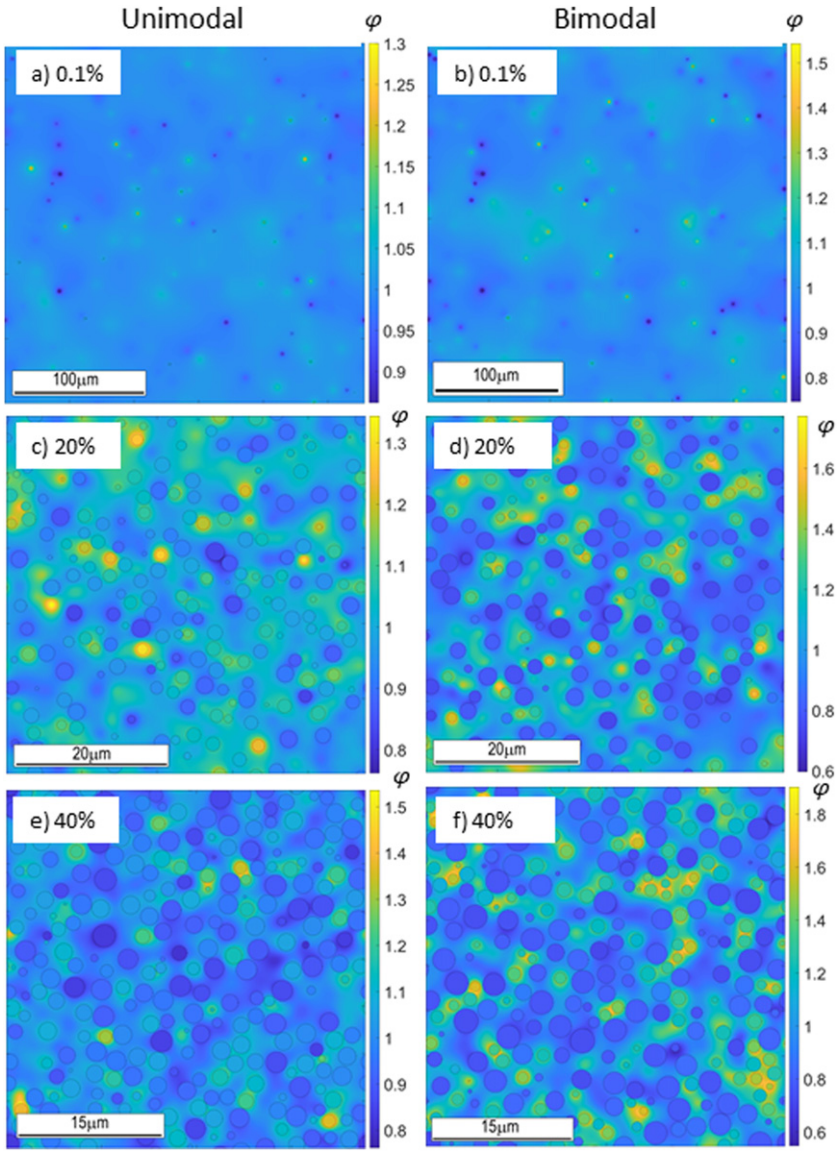

Figure 3. The dimensionless diffusion potential for a unimodal and bimodal dispersions with volume fractions of 0.1%, 20% and 40%.

volume fraction, and is a function of the spatial arrangement and polydispersity of the particle phase. This behaviour is what the $z(r, t)$ factor in the particle growth rate (see equation (4)) aims to capture.

Figure 4 compares the particle growth rates calculated using the WGRV discrete particle model to the MR, SF, Ardell, and Di Nunzio models. As expected, the WGRV model predicts particle growth rates dependent on the local environment of the precipitate, which is determined by the spatial distribution of neighbouring precipitates. The contour plot in figure 4 describes the variation in particle growth rates for a particle of a given size. It can be seen that all models

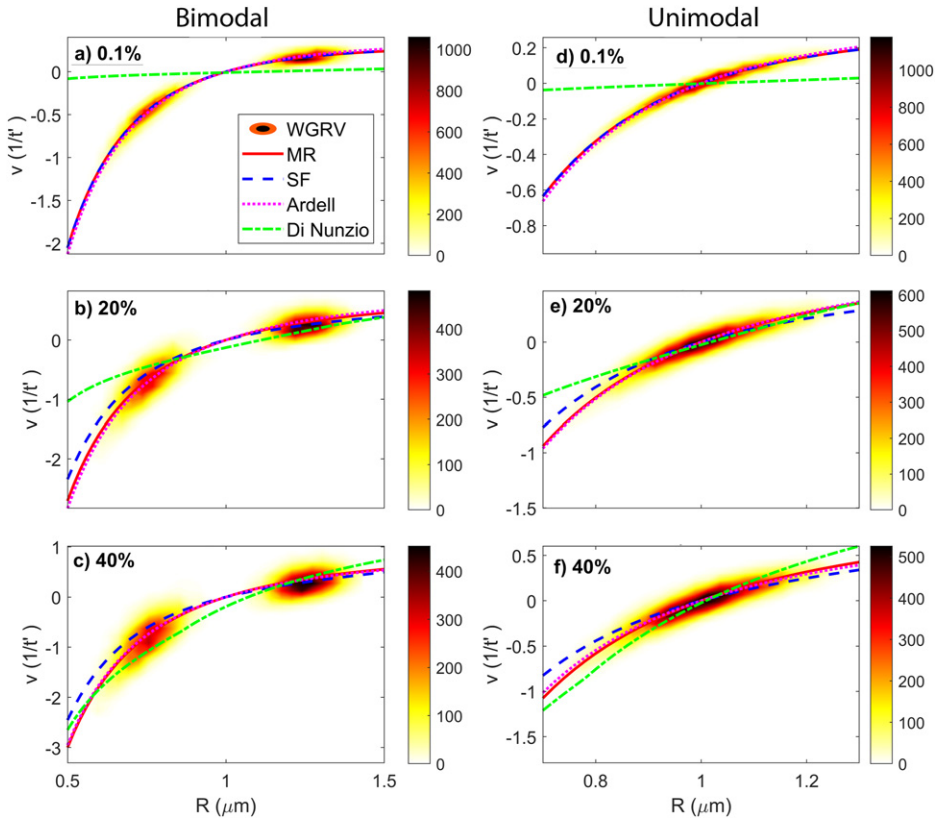

Figure 4. A comparison of the predicted particle growth rates for bimodal and unimodal dispersions with different volume fractions. The WGRV model predicts a range of growth rates for a given particle size. This range is presented with a normalised continuous bivariate distribution function with the magnitude of the density given in the colour bar. The WGRV particle growth rates are compared against those calculated using the MR, SF, Ardell, and Di Nunzio particle growth rates summarised in equations (21)–(24), respectively.

except for Di Nunzio's model capture correct dilute particle behaviour (volume fraction 0.1%), where $z \approx 1$. The MR and Ardell models are within the range of growth rates predicted by the WGRV model and offer a good description of the mean particle growth rate when compared to the WGRV model, demonstrating that assumptions used in these models are reasonable. The SF z factor does not capture the accelerated kinetics for non-dilute volume fractions of particles. The results have used a value of 2.0 for the parameter k in equation (22), which was found to be the limit for the PRDs of interest before the onset of numerical instability considering the kinetics of the bimodal dispersion.

Although the Ardell and MR descriptions of z follow the correct behaviour, they underestimate the rate of particle coarsening predicted by the WGRV model for particle dispersions with a volume fractions of 40%, as shown in figure 5. Marqusee and Ross [14] developed their description considering particle volume fractions as high as 10%. Figures 4 and 5 show it is suitable for 20% volume fractions; however, both the MR and Ardell's z factors fail to capture the accelerated rate of particle coarsening predicted by the WGRV model for the dispersions

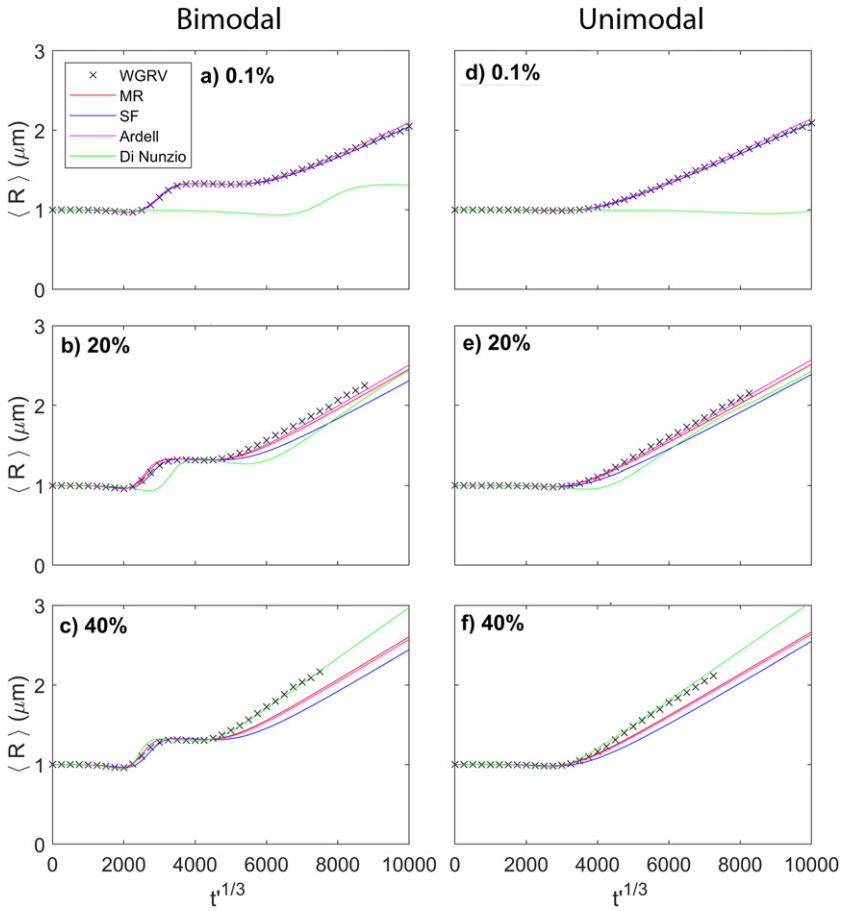

Figure 5. A comparison of the predicted mean particle radius during particle coarsening considering a bimodal and unimodal dispersion with varying volume fractions. The crosses refer to the behaviour predicted by the WGRV model, with the continuous lines describing the statistical calculations. The behaviour is presented in normalised time scaled to the power of a third.

containing a volume fraction of 40%. The z factor approximation following Ardell's approach does not currently offer a substantial benefit compared to the MR z factor and requires greater computation time. As a result, the Marqusee and Ross [14] z factor is the most suitable out of the descriptions examined in this work. Di Nunzio's pairwise interaction model [13] predicts too slow kinetics of the dispersions with 0.1% and 20% volume fraction, however captures the kinetics of the 40% dispersion accurately.

4.2. Isothermal aging of IN738LC

The discrete particle WGRV model and mean-field models with the MR z factor and Di Nunzio's particle growth rate have been applied to predict the coarsening kinetics of γ' precipitates in the nickel-based superalloy Inconel 738LC. Validation of model predictions will be made against experimental data presented by Anderson *et al* [19] on the isothermal aging

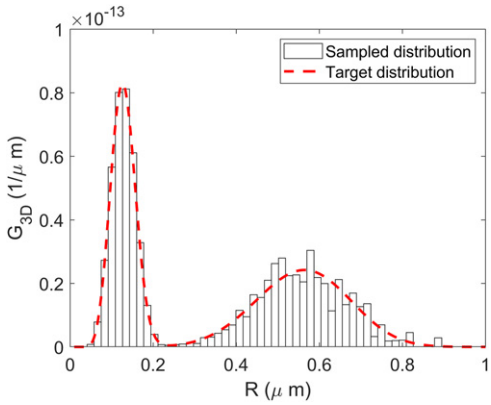

Figure 6. The as-heat treated γ' precipitate distribution in Inconel 738LC.

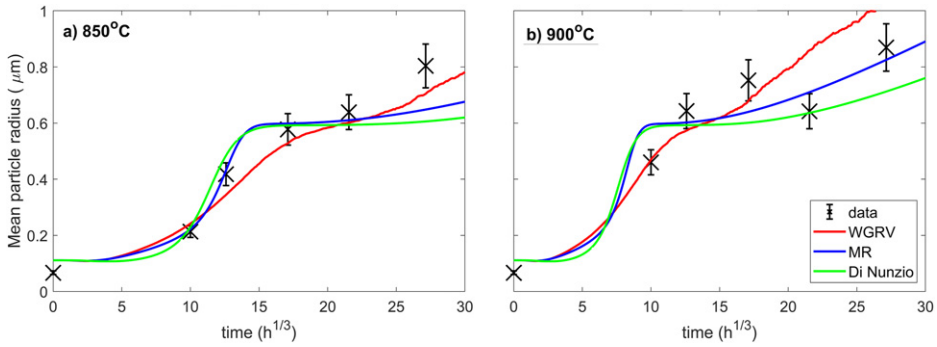

Figure 7. The evolution of the mean particle radius during isothermal aging of IN738LC comparing experimental data with the WGRV discrete particle model and mean-field models using the MR z correction factor and Di Nunzio's particle growth rate.

of IN738LC at 850 °C and 900 °C. The initial bimodal particle size distribution is shown in figure 6. The parameters used in the calculation are given in table 1 for the WGRV and MR models, and table 2 for the Di Nunzio model.

A comparison of the measured and predicted evolution of the mean particle radius is given in figure 7. The two particle populations shown in figure 6 will be referred to as secondary and tertiary particles, respectively. The MR and Di Nunzio models predict a more pronounced slowing of the growth of the mean particle radius upon dissolution of the tertiary particle population. Once the tertiary particles are predicted to be fully dissolved, the secondary particle size distribution changes shape so that there is a larger left-hand tail to the dispersion due to dissolving secondary particles. Whilst the secondary dispersion changes shape, there is a slowing in the growth of the mean particle radius. The WGRV model predicts a much less pronounced reduction in the growth of the mean particle radius. This is due to the location specific kinetics resulting in the dissolution of secondary particles and the growth of some tertiary particles based upon the relative sizes of neighbouring particles.

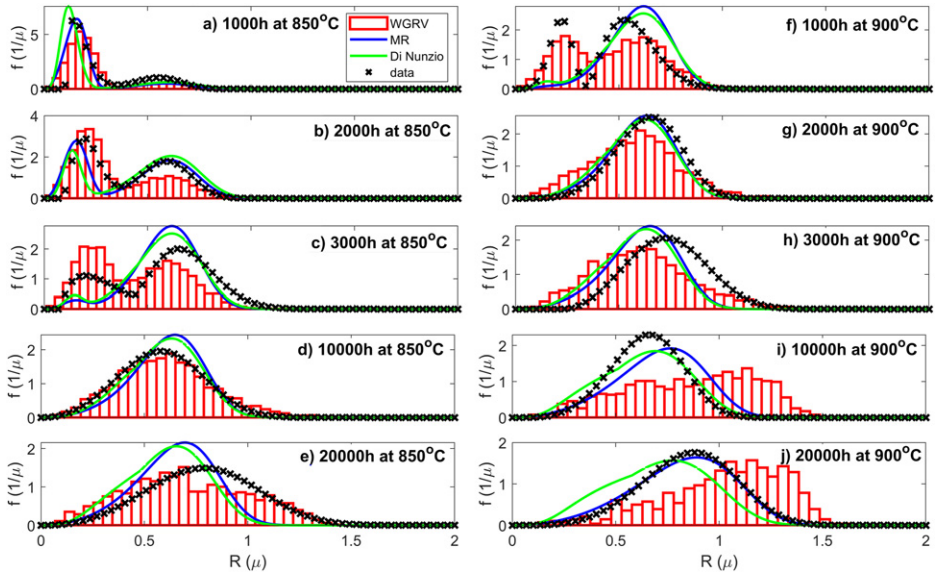

Figure 8. A comparison of the measured and predicted particle size distributions during isothermal aging at 850 °C and 900 °C of IN738LC. The experimental data is presented with crosses. A histogram is used to present the results from the discrete WGRV model. Blue and green continuous distributions describe the results from the MR z factor model and Di Nunzio's particle growth rate, respectively.

The transition from a bimodal to unimodal distribution obtained from the WGRV model is closer to the experimental data compared to the MR and Di Nunzio calculations, which is more clearly observed when examining the distributions shown in figure 8. The MR z factor appears to better capture the transition from bimodal to unimodal in comparison to Di Nunzio's model in this case.

4.3. Isothermal aging of coarse grain RR1000

The precipitation models have also been applied to simulate the isothermal aging kinetics in the coarse grain nickel superalloy RR1000. The initial bi-modal PRD including secondary and tertiary precipitates is presented in figure 9. The parameters used in the calculation are given in table 1 for the WGRV and MR models, and table 2 for the Di Nunzio model.

Figure 10 compares the predicted volume fraction of tertiary and secondary γ' precipitates during isothermal aging at 700 °C, 750 °C, and 800 °C. At 700 °C, the data suggests a slight increase in volume fraction of tertiary γ' at the expense of secondary particles, which is not captured by none of the models investigated in this study. All models predict the reduction in volume fraction of tertiary particles for the three temperatures under consideration. At 750 °C, experimental measurements indicate a reduction in the tertiary γ' volume fraction; however tertiary particles remain in the dispersion after 500 h. The WGRV model captures the tertiary behaviour after 100 h reasonably well, although for times less that 100 h it predicts a much faster dissolution rate than suggested by the data. The mean-field models predict rapid dissolution of the tertiary at this temperature, dissolving completely within 200 h. At 800 °C, the data indicates the rapid dissolution of tertiary γ'; however, the mean-field models over-predict the dissolution kinetics whilst the direct numerical simulation of the growth rates captures the

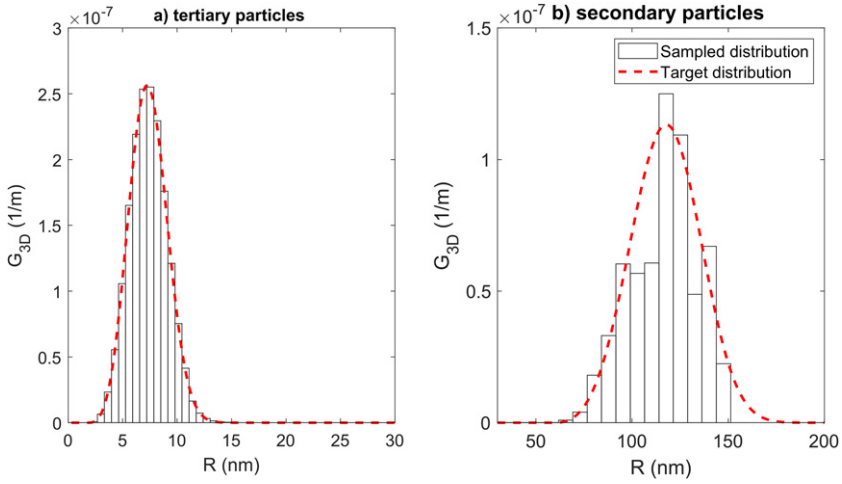

Figure 9. The as-heat treated γ' precipitate distribution in RR1000.

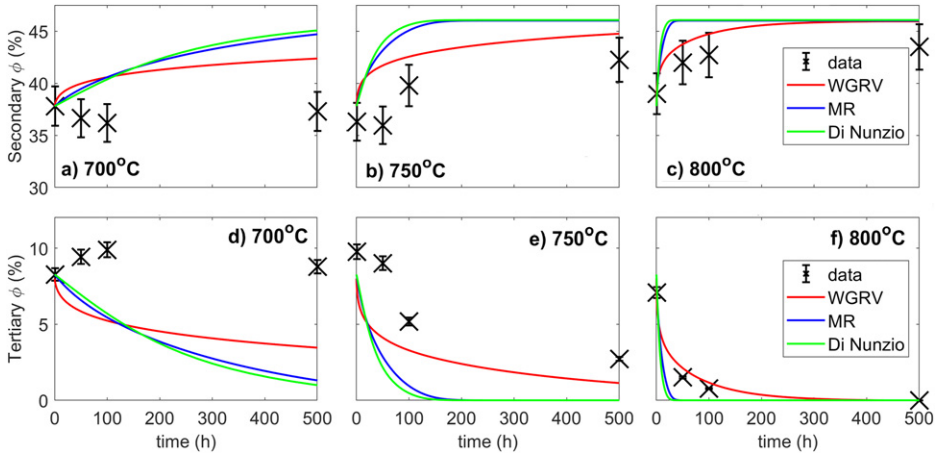

Figure 10. A comparison of the measured and predicted evolution the volume fraction of secondary and tertiary particles at temperatures of 700 °C, 750 °C, and 800 °C within coarse grain RR1000. The data is compared against model predictions from the mean-field and discrete WGRV models. Figures (a)–(c) present results for the secondary precipitates, and figures (d)–(f) present results for tertiary particles.

dissolution of tertiary with reasonable accuracy. It can be seen that the WGRV model better captures the dissolution kinetics of the tertiary γ' precipitates during isothermal aging.

Figure 11 compares the predicted and measured PRDs during isothermal aging. The WGRV model predicts the mean size of tertiary with reasonable accuracy at 700 °C and 800 °C, however overestimates the growth rate of tertiary at 750 °C.

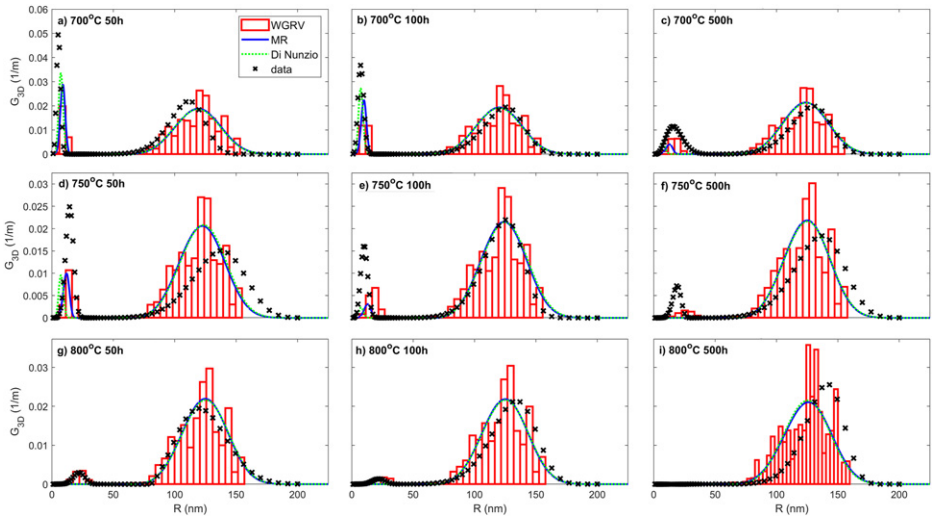

Figure 11. A comparison of the measured and predicted particle size dispersions during isothermal aging at 700 °C, 750 °C, and 800 °C of RR1000 comparing the mean-field and WGRV discrete particle model to measured PRDs.

5. Discussion

Direct numerical solutions obtained in this study suggest that the Marqusee and Ross [14] and Ardell [8] approximation using the Lu and Torquato [24] nearest neighbour distribution function provides a reasonable correction factor for volume fractions up to 20%. The z factors fail to capture the accelerated rate of precipitation predicted by the WGRV model at higher volume fractions. Di Nunzio's model [13] captures the kinetics of dispersions with 40% volume fraction, however, it deviates considerably from the WGRV model at lower volume fractions. This limitation is an issue when modelling nucleation and growth of particles, or dissolution during service or manufacture.

When comparing model predictions with experimental data, the WGRV model gives the best agreement, with improved predictions of the transition from a bimodal to a unimodal dispersion. The mean-field statistical models predict a rapid change from bimodal to unimodal dispersion, followed by a low growth rate period before reaching the attractor state, as shown in figure 7. During this transition, the mean size is not changing substantially while the width of the distribution is getting wider.

The WGRV model predicts growth for a fraction of particle belonging to smaller population, whilst the mean-field approximations predicts that all particles smaller than the critical radius dissolve. This is significant in RR1000, where the WGRV captures the increased stability of the tertiary particle population where the mean-field model suggests they should dissolve from the onset of coarsening. The ability to predict tertiary kinetics correctly is important when modelling service conditions, as tertiary precipitates significantly influence creep behaviour of powder disc alloys [28]. Although the WGRV model captures the stability of tertiary particles, their predicted size is greater than those observed experimentally after isothermal aging at 750 °C as shown in figure 11(e). The predicted dissolution in tertiary particles shown in figures 10(d) and (e) differs to the measured data. For example, in figure 10(e) the reduction of the tertiary volume fraction appears sigmoidal, compared to the predicted exponential

decay. At 800 °C, the data and models agree with exponential decay like behaviour. There are many factors that could contribute to the differences in dissolution kinetics predicted at lower temperatures.

One possibility is that the approximation of steady-state diffusion applies at 800 °C, where diffusivities and kinetics are sufficient so that steady-state diffusion fields are quickly reached. None of the models investigated account for differences in chemistry between precipitates, which can be significant in as-quenched nickel superalloys [29, 30]. The chemical driving force for precipitation and the interfacial energy would vary with precipitate composition [31], altering the coarsening behaviour of the particle populations. The assumption that the diffusion fields are quasi-static is unlikely to be accurate when considering precipitates which vary significantly in composition, with differences in matrix composition surrounding the different populations of particles. Radis *et al* [32] observed solute depletion zones around particle populations in the quenched nickel superalloy UDIMET 720 [32]. Anderson *et al* [20] used such depletion zones to justify a phenomenological model where isolated tertiary precipitates do not compete directly with secondary particles until the matrix has sufficiently homogenised. The model succeeds in capturing the increased stability of the tertiary particles in RR1000, however it would not help with IN738LC where the larger tertiary particles are unlikely to remain isolated at the elevated temperatures of interest.

Yang *et al* [33] have further developed the WGRV model to account for spatially varying alloy chemistry in the vicinity of grain boundaries. A similar approach needs to be developed to account for differences in composition between secondary and tertiary precipitates if transient behaviour associated with non-equilibrium conditions is to be simulated correctly. The diffusion fields surrounding secondary and tertiary particles with significant composition differences cannot be adequately approximated as a steady-state problem.

The current model formulations are based upon a pseudo-binary approximation of the alloy chemistry, grouping γ' forming elements, similar to the approaches of Coakley *et al* [34] and Semiatin *et al* [35]. Multi-component descriptions provide a more realistic description of the alloys of interest. Appropriate mobility databases can be used to determine diffusivities as a function of alloy composition. Svoboda *et al* [36] have applied the thermodynamic extremal principle to derive a multi-component description of a steady-state point source/sink model of competitive growth. Although this is an improvement, it does not directly address the challenges in capturing the coarsening and dissolution kinetics observed in tertiary precipitates in RR1000 at temperatures of $\leqslant$750 °C.

The models do not consider changes to precipitate morphology induced by either energy minimisation of interfacial and elastic energies [37, 38], or through precipitate coalescence events [39]. Elastically induced morphology changes would slow the growth rate of the precipitates, whilst coalescence events would rapidly increase the size of the agglomerating precipitates. Figure 10(d) shows that at 700 °C, the data suggests a slight increase in volume fraction of tertiary γ', which is not captured by either mean-field or WGRV models. One possibility is that during these conditions the matrix is still supersaturated and that the volume fraction of γ' is still growing, delaying the dissolution of the tertiary precipitates. This behaviour could be attributed to experimental error, however another explanation is inverse coarsening as described by Su *et al* [40], where small particles are able to grow at the expense of larger particles as their location is less elastically distorted than the neighbouring larger particle. Kawasaki and Enomoto [41] developed a statistical model that accounts for inverse coarsening behaviour which can be introduced into the WGRV model. They approximate the total mean interaction energy of a particle by the summation of the pair-wise interaction energies as described by Eshelby [42] between the reference particle and every other particle within the domain [41]. The mean elastic interaction energy may be included within the Gibbs–Thomson equation

when calculating the matrix composition at the precipitate-matrix interface. The alloys investigated in this work do not exhibit significant shape changes during coarsening, remaining globular, however in other conditions or alloys with higher elastic misfit between the particle and matrix phases, the approach of Kawasaki and Enomoto [41] might be useful. This approach does not account for the migration of the particle's centre [43], or elastic energy induced changes in particle morphology [38]. Onuki and Nishimori [44] found that during particle coarsening, changes to particle morphology minimise the elastic interaction energy meaning that the elastic interaction energy calculated from Eshelby [42] would over estimate this effect.

Even without accounting for the elastic interaction energy, the WGRV model offers an improvement to conventional mean-field models when modelling the coarsening kinetics of IN738LC and can capture the unexpected stability exhibited by tertiary particles during isothermal aging of RR1000. This work has focused on competitive growth in nickel-based superalloys; however, the findings are relevant to modelling precipitates in other alloy systems, such as aluminium alloys [10, 33], steel [45], and zirconium alloys [46].

Statistical models provide the means of predicting important microstructural information at time scales and length scales relevant to both processing and alloy performance. They can be readily incorporated into process models to provide location specific property prediction [47], and can be used to predict mechanical properties. They are limited by their reduced accuracy caused by the many simplifying assumptions made in their derivation. This work shows that addressing issues with regards to competitive growth can improve predicted behaviour within the transient Ostwald ripening regime.

6. Conclusion

A number of approximations of competitive growth used in mean-field particle coarsening theory have been assessed against the WGRV multi-particle model. The results are relevant to conditions where it is reasonable to assume quasi-static diffusion fields with spherical particle geometry. It is shown that the MR $z(R, t)$ factor and Ardell's $z(R, t)$ factor capture the predicted behaviour of the discrete WGRV model for volume fractions up to 20%, however under-predict the kinetics of higher volume fractions. Di Nunzio's pairwise interaction model behaves well at 40% but does not extrapolate to lower volume fraction dispersions, and does not reproduce the experimentally observed coarsening kinetics as closely as the MR correction factor considering the two multi-modal nickel based superalloys studied in this work. The multi-particle WGRV model captures the coarsening kinetics observed in the aging of as-heat treated Inconel 738LC, and predicts the unexpected stability of tertiary particles in the coarsening of as-heat treated coarse grain RR1000, despite the simplifying assumptions regarding the particle morphology and the treatment of a multi-component alloy as a pseudo-binary alloy. This work demonstrates that statistical models can be improved by focusing on the description of competitive growth where dissolution or growth is determined by the local environment rather than a global critical particle radius.

Data availability statement

The data that support the findings of this study are available upon reasonable request from the authors.

Appendix A. Lu and Torquato nearest neighbour particle spacing

The mean particle radius used to define the diffusion screening length has been approximated by Torquato's nearest neighbour distribution function [48], considering randomly arranged 3D spherical polydisperse non-penetrating particles.

Consider a reference particle within the dispersion with radius R_f. The likelihood that a sphere centred on the reference particle with radius λ is free of neighbouring particle centres is given by the $E_\mathrm{p}(R_\mathrm{f}, \lambda)$ function. For $\lambda < R_\mathrm{f}$, the volume considered is within the reference particle, so $E_\mathrm{p}(R_\mathrm{f}, \lambda) = 1$. As $\lambda > R_\mathrm{f}$, the likelihood of encountering another particle increases. When $E_\mathrm{p}(R_\mathrm{f}, \lambda)$ decays to zero, this describes the distance where another particle centre will definitely be encountered within the volume of radius λ. The mean nearest neighbour matrix spacing for the reference particle is thus

$$\langle \lambda \rangle = \int_{R_\mathrm{f}}^{\infty} E_\mathrm{p}\, \mathrm{d}\lambda \tag{26}$$

The E_p function is given by

$$E_\mathrm{p}(R_\mathrm{f}, \lambda) = \frac{E_v(\lambda)}{E_v(R_\mathrm{f})} \tag{27}$$

where the E_v function is calculated using a normalised exclusion zone distance x

$$x = \frac{\lambda}{\langle D \rangle}, \tag{28}$$

where $\langle D \rangle = 2\langle R \rangle$. The exclusion volume $E_v(x)$ is

$$E_v(x) = \eta\, \exp\left[-2\eta S\left(a_0 x^3 + a_1 x^2 + a_2 x\right)\right] \tag{29}$$

where η is the volume fraction, S is the specific surface, and a_0, a_1, and a_2 are coefficients. Let $f = F/N_v$, so that f is a probability density distribution function descriptive of the size distribution of particles. Let the Dth moment of $f(R,t)\mathrm{d}R$ be given by

$$\langle R^{(D)} \rangle = \int_0^{\infty} f R^{(D)}\, \mathrm{d}R \tag{30}$$

The specific surface is defined as

$$S = \frac{\langle R^2 \rangle}{\langle R^3 \rangle} \langle R \rangle \tag{31}$$

The coefficients a_0, a_1, and a_2 are

$$\begin{aligned} a_0 &= \frac{4\left(\langle R \rangle^2 / \langle R^2 \rangle\right)(1-\eta)(1-\eta+3\eta S) + 8\eta^2 S^2}{(1-\eta)^3} \\ a_1 &= \frac{6\left(\langle R \rangle^2 / \langle R^2 \rangle\right)(1-\eta) + 9\eta S}{(1-\eta)^2} \\ a_2 &= \frac{3}{1-\eta} \end{aligned} \tag{32}$$

The reference particle used in the calculation is the mean particle radius, $\langle R\rangle$, and the diffusion screening distance is approximated as $\langle\lambda\rangle$.

Appendix B. Reformulation of Di Nunzio's model

Di Nunzio's discrete model utilising multiple pairwise interactions to capture competitive growth is given below [13]

$$\begin{aligned} V(R_i,t) &= \sum_{j=1}^{n} \frac{A}{R_i^2}\frac{\phi^{1/3}}{1-\phi^{1/3}}\frac{\langle R^2\rangle}{\langle R\rangle}\frac{\tilde{v}_i\tilde{v}_j}{\langle\tilde{v}\rangle^2}\frac{n_j}{N_v}\left(\frac{1}{R_j}-\frac{1}{R_i}\right)\\ \tilde{v}_i &= \left(\tilde{\alpha}_i^3-1\right)\frac{R_i^3}{\langle R^3\rangle}+1\\ \tilde{\alpha}_i^3 &= \alpha^2\frac{\langle R^3\rangle}{\langle R^2\rangle}\frac{\phi^{-2/3}}{R_i}+1\\ \langle\tilde{v}\rangle &= \sum_{j=1}^{n} n_j\tilde{v}(R_j)\\ A &= \frac{D\gamma V_{\mathrm{m}}c_0}{R_{\mathrm{g}}T}\\ \langle R^D\rangle &= \sum_{j=1}^{n} n_j R_j^D, \end{aligned} \tag{33}$$

where fraction of particles within the size class of R_i is given by n_i. This model may be expressed using the continuous distribution function $\mathcal{F}$ using the relationship $n_i = \mathcal{F}(R,t)\mathrm{d}R$ so that the averaged moments $\langle R^D\rangle$ is given by

$$\langle R^D\rangle = \sum_{j=1}^{n} n_j R_j^D \equiv \frac{1}{M^0}\int_0^\infty \mathcal{F}(R)R^D\mathrm{d}R \equiv \frac{M^D}{M^0}, \tag{34}$$

where M^D refers to the Dth moment of $\mathcal{F}(R,t)$ as shown in equation (1). The following equation set is obtained when expressing equation set 35 in terms of the continuous distribution function $\mathcal{F}$ and moments defined in equation (1).

$$\begin{aligned} V(R_i,t) &= \frac{A}{R_i^2}\frac{\phi^{1/3}}{1-\phi^{1/3}}\frac{M^2}{M^1}\tilde{b}(R_i)M^0\int_0^\infty \tilde{b}(R_j)\mathcal{F}(R_j,t)\left(\frac{1}{R_j}-\frac{1}{R_i}\right)\mathrm{d}R_j\\ \tilde{b}(R_i) &= \frac{\tilde{v}(R_i)}{\int_0^\infty F(R)\tilde{v}(R)\mathrm{d}R}\\ \tilde{v}(R_i) &= 1+\alpha^2M^0\frac{R_i^2}{M^2}\frac{1}{\phi^{2/3}} \end{aligned} \tag{35}$$

ORCID iDs

M J Anderson https://orcid.org/0000-0001-5552-4459

L Liao https://orcid.org/0000-0003-3052-6671

H C Basoalto https://orcid.org/0000-0002-2102-914X

References

[1] Deschamps A and Hutchinson C R 2021 Precipitation kinetics in metallic alloys: experiments and modeling *Acta Mater.* **220** 117338
[2] Coakley J, Dye D and Basoalto H 2011 Creep and creep modelling of a multimodal nickel-base superalloy *Acta Mater.* **59** 854–63
[3] Galindo-Nava E I, Connor L D and Rae C M F 2015 On the prediction of the yield stress of unimodal and multimodal γ' nickel-base superalloys *Acta Mater.* **98** 377–90
[4] Fang Q, Li L, Li J, Wu H, Huang Z, Liu B, Liu Y and Liaw P K 2019 A statistical theory of probability-dependent precipitation strengthening in metals and alloys *J. Mech. Phys. Solids* **122** 177–89
[5] Greenwood G W 1956 The growth of dispersed precipitates in solutions *Acta Metall.* **4** 243–8
[6] Lifshitz I M and Slyozov V V 1961 The kinetics of precipitation from supersaturated solid solutions *J. Phys. Chem. Solids* **19** 35–50
[7] Wagner C 1961 Theorie der alterung von niederschlagen durch umlonsen (Ostwald-reifung) *Z. Elektrochem. Phys. Chem.* **65** 581–91
[8] Ardell A J 1972 The effect of volume fraction on particle coarsening: theoretical considerations *Acta Metall.* **20** 61–71
[9] Tsumuraya K and Miyata Y 1983 Coarsening models incorporating both diffusion geometry and volume fraction of particles *Acta Metall.* **31** 437–52
[10] Wang K, Glicksman M and Lou C 2006 Correlations and fluctuations in phase coarsening *Phys. Rev.* E **73** 061502
[11] Glicksman M E, Wang K-G and Marsh S P 2001 Diffusional interactions among crystallites *J. Crystallogr. Growth* **230** 318–27
[12] Svoboda J and Fischer F D 2014 Generalization of the Lifshitz–Slyozov–Wagner coarsening theory to non-dilute multi-component systems *Acta Mater.* **79** 304–14
[13] Di Nunzio P E 2018 A discrete model of Ostwald ripening based on multiple pairwise interactions *Phil. Mag.* **98** 1674–95
[14] Marqusee J A and Ross J 1984 Theory of Ostwald ripening—competitive growth and its dependence on volume fraction *J. Chem. Phys.* **80** 563–43
[15] Voorhees P W and Glicksman M E 1984 Solution to the multi-particle diffusion problem with applications to Ostwald ripening: I. theory *Acta Metall.* **32** 2001–11
[16] Hayakawa H and Family F 1990 Many-body effects in two-dimensional Ostwald ripening *Physica* A **163** 491–500
[17] Wang K G, Glicksman M E and Rajan K 2004 Modeling and simulation for phase coarsening: a comparison with experiment *Phys. Rev.* E **69** 061507
[18] Chen M K and Voorhees P W 1993 The dynamics of transient Ostwald ripening *Modelling Simul. Mater. Sci. Eng.* **1** 591–612
[19] Anderson M J, Rowe A, Wells J and Basoalto H C 2016 Application of a multi-component mean field model to the coarsening behaviour of a nickel-based superalloy *Acta Mater.* **114** 80–96
[20] Anderson M J, Schulz F, Lu Y, Kitaguchi H S, Bowen P, Argyrakis C and Basoalto H C 2020 On the modelling of precipitation kinetics in a turbine disc nickel based superalloy *Acta Mater.* **191** 81–100
[21] Davies C K L, Nash P and Stevens R N 1980 Effect of volume fraction of precipitate on Ostwald ripening *Acta Metall.* **28** 179–89
[22] Wang K G, Glicksman M E and Rajan K 2005 Length scales in phase coarsening: theory, simulation, and experiment *Comput. Mater. Sci.* **34** 235–53
[23] Bansal P P and Ardell A J 1972 Average nearest-neighbor distances between uniformly distributed finite particles *Metallography* **5** 97–111

[24] Lu B and Torquato S 1992 Nearest-surface distribution-functions for polydispersed particle-systems *Phys. Rev.* A **45** 5530–44
[25] Wang K G and Glicksman M E 2015 Phase coarsening in thin films *JOM* **67** 1905–12
[26] Anderson M J, Panwisawas C, Sovani Y, Turner R P, Brooks J W and Basoalto H C 2018 Mean-field modelling of the intermetallic precipitate phases during heat treatment and additive manufacture of Inconel 718 *Acta Mater.* **156** 432–45
[27] Anderson M J, Rowe A, Wells J and Basoalto H C 2016 Application of a multi-component mean field model to the coarsening behaviour of a nickel-based superalloy *Acta Mater.* **114** 80–96
[28] Locq D, Caron P, Raujol S, Pettinari-Sturmel F, Coujou A and Clément N 2004 On the role of tertiary γ' precipitates in the creep behaviour at 700 °C of a pm disk superalloy *Superalloys*
[29] Chen Y Q, Slater T J A, Lewis E A, Francis E M, Burke M G, Preuss M and Haigh S J 2014 Measurement of size-dependent composition variations for gamma prime (γ') precipitates in an advanced nickel-based superalloy *Ultramicroscopy* **144** 1–8
[30] Singh A R P, Nag S, Chattopadhyay S, Ren Y, Tiley J, Viswanathan G B, Fraser H L and Banerjee R 2013 Mechanisms related to different generations of γ' precipitation during continuous cooling of a nickel base superalloy *Acta Mater.* **61** 280–93
[31] Sheng Z, Rolland M, Zhou T, Odqvist J and Hedström P 2021 Langer–Schwartz–Kampmann–Wagner precipitation simulations: assessment of models and materials design application for Cu precipitation in PH stainless steels *J. Mater. Sci.* **56** 1–22
[32] Radis R, Schaffer M, Albu M, Kothleitner G, Pölt P and Kozeschnik E 2009 Multimodal size distributions of γ' precipitates during continuous cooling of UDIMET 720 Li *Acta Mater.* **57** 5739–47
[33] Yang N, Saidi P, Daymond M R and Hoyt J J 2017 Modeling of particle coarsening and precipitation free zones *Model. Simul. Mater. Sci. Eng.* **25** 085012
[34] Coakley J, Basoalto H and Dye D 2010 Coarsening of a multimodal nickel-base superalloy *Acta Mater.* **58** 4019–28
[35] Semiatin S L, Kim S-L, Zhang F and Tiley J S 2015 An investigation of high-temperature precipitation in powder-metallurgy, gamma/gamma-prime nickel-base superalloys *Metall. Mater. Trans.* A **46** 1715–30
[36] Svoboda J, Shan Y V, Zickler G A, Kozeschnik E and Fischer F D 2020 Local approach for coarsening of precipitates *Scr. Mater.* **178** 232–5
[37] Doi M 1992 Coarsening behaviour of coherent precipitates in elastically constrained systems *Mater. Trans. JIM* **33** 637–49
[38] Thompson M E, Su C S and Voorhees P W 1994 The equilibrium shape of a misfitting precipitate *Acta Metall. Mater.* **42** 2107–22
[39] Basoalto H and Anderson M 2016 An extension of mean-field coarsening theory to include particle coalescence using nearest-neighbour functions *Acta Mater.* **117** 122–34
[40] Su C H and Voorhees P W 1996 The dynamics of precipitate evolution in elastically stressed solids: I. Inverse coarsening *Acta Mater.* **44** 1987–99
[41] Kawasaki K and Enomoto Y 1988 Statistical theory of Ostwald ripening with elastic field interaction *Physica* A **150** 463–98
[42] Ardell A J and Nicholson R B 1966 On the modulated structure of aged Ni–Al alloys *Acta Metall.* **14** 1295–309
[43] Imaeda T and Kawasaki K 1990 Multipole expansion in the Ostwald ripening theory *Physica* A **164** 335–52
[44] Onuki A and Nishimori H 1991 On Eshelby's elastic interaction in two-phase solids *J. Phys. Soc. Japan* **60** 1–4
[45] Wang K G, Guo Z, Sha W, Glicksman M E and Rajan K 2005 Property predictions using microstructural modeling *Acta Mater.* **53** 3395–402
[46] Xia L, Chen D, Cao Y, Xiao X and Jiang C 2021 High temperature nano-indentation on the mechanical properties of Zr and Zr–Fe alloys: experimental and theoretical analysis *Mech. Mater.* **162** 104053
[47] Basoalto H C, Panwisawas C, Sovani Y, Anderson M J, Turner R P, Saunders B and Brooks J W 2018 A computational study on the three-dimensional printability of precipitate-strengthened nickel-based superalloys *Proc. R. Soc.* A **474** 20180295
[48] Torquato S 1988 *Random Heterogeneous Materials* (Berlin: Springer)